Supplementary Information

Stability of multifunctional Pd–Rh electrocatalysts supported on $Co_3O_4(111)$ in alkaline environment: Impact of the electronic metal–support interaction

Alexander Simanenko[1], Jan Škvára[2], Pankaj Kumar Samal,[2] Evanie Franz[1], Robert Hübsch[1], Tomáš Skála[2], Nataliya Tsud[2], Sascha Mehl[3], Daniel Schauermann,[1] Viktor Johánek[2], Josef Mysliveček[2], Olaf Brummel[1], Yaroslava Lykhach[1,*], Jörg Libuda[1]

[1]Interface Research and Catalysis, ECRC, Friedrich-Alexander-Universität Erlangen-Nürnberg, Egerlandstraße 3, 91058 Erlangen, Germany

[2]Charles University, Faculty of Mathematics and Physics, Department of Surface and Plasma Science, V Holešovičkách 2, Prague, 18000, Czech Republic

[3]Elettra-Sincrotrone Trieste SCpA, Strada Statale 14, km 163.5, Basovizza-Trieste, 34149, Italy

E-mail address: yaroslava.lykhach@fau.de

S1. Fitting parameters for Pd 3d and Rh 3d spectra

The fitting parameters for the Pd 3d and Rh 3d spectra obtained from Pd/Co_3O_4(111), Rh/Co_3O_4(111), Rh@Pd/Co_3O_4(111) and Pd@Rh/Co_3O_4(111) in Tables S1-S4. Note that the width of the Pd 3d and Rh 3d spectra are specific for the X-ray source and photon energy used during the data acquisition (MSB, Elettra, May 24 – 31, 2023).

Table S1. The fitting parameters for the Pd 3d spectra obtained with photon energy 410 eV from as-prepared Pd/Co_3O_4(111) model catalyst. The parameters include the binding energy (BE), spin-orbit splitting (SOS), branching ratio of peak areas in the doublet (BR), widths at half maximum (WHM) for Lorentzian (L-WHM) and Gaussian (G-WHM) contributions in the Doniach–Šunjić function convoluted with a Gaussian profile, asymmetry parameter of the Lorentzian contribution (AP).

Contribution	BE ($3d_{5/2}$), eV	SOS, eV	BR	L-WHM, eV	G-WHM, eV	AP
Pd^0,	335.34	5.3	1.5	0.3	1.0	0.07

Table S2. The fitting parameters for the Rh 3d spectra obtained with photon energy 410 eV from as-prepared Rh/Co_3O_4(111) model catalyst. The parameters include the binding energy (BE), spin-orbit splitting (SOS), branching ratio of peak areas in the doublet (BR), widths at half maximum (WHM) for Lorentzian (L-WHM) and Gaussian (G-WHM) contributions in the Doniach–Šunjić function convoluted with a Gaussian profile, asymmetry parameter of the Lorentzian contribution (AP).

Contribution	BE ($3d_{5/2}$), eV	SOS, eV	BR	L-WHM, eV		G-WHM, eV		AP
				$3d_{5/2}$	**$3d_{3/2}$**	**$3d_{5/2}$**	**$3d_{3/2}$**	
Rh^0	307.13	4.7	1.5	0.3	0.3	0.7	1.0	0.09
Rh^{3+}	308.23	4.7	1.5	0.4	0.4	1.0	1.3	0.00

Table S3. The fitting parameters for the Pd 3d and Rh 3d spectra obtained with photon energy 410 eV from as-prepared Rh@Pd/Co_3O_4(111) model catalyst. The parameters include the binding energy (BE), spin-orbit splitting (SOS), branching ratio of peak areas in the doublet (BR), widths at half maximum (WHM) for Lorentzian (L-WHM) and Gaussian (G-WHM) contributions in the

Doniach–Šunjić function convoluted with a Gaussian profile, asymmetry parameter of the Lorentzian contribution (AP).

Contribution	BE ($3d_{5/2}$), eV	SOS, eV	BR	L-WHM, eV	G-WHM, eV	AP
Pd^0,	335.34	5.3	1.5	0.4	0.9	0.07

Contribution	BE ($3d_{5/2}$), eV	SOS, eV	BR	L-WHM, eV		G-WHM, eV		AP
				$3d_{5/2}$	**$3d_{3/2}$**	**$3d_{5/2}$**	**$3d_{3/2}$**	
Rh^0	307.15	4.7	1.5	0.3	0.3	0.8	1.0	0.07
Rh^{3+}	308.25	4.7	1.5	0.4	0.4	1.1	1.4	0.00

Table S4. The fitting parameters for the Pd 3d and Rh 3d spectra obtained with photon energy 410 eV from as-prepared Pd@Rh/Co_3O_4(111) model catalyst. The parameters include the binding energy (BE), spin-orbit splitting (SOS), branching ratio of peak areas in the doublet (BR), widths at half maximum (WHM) for Lorentzian (L-WHM) and Gaussian (G-WHM) contributions in the Doniach–Šunjić function convoluted with a Gaussian profile, asymmetry parameter of the Lorentzian contribution (AP).

Contribution	BE ($3d_{5/2}$), eV	SOS, eV	BR	L-WHM, eV	G-WHM, eV	AP
Pd^0,	335.30	5.3	1.5	0.4	0.8	0.07

Contribution	BE ($3d_{5/2}$), eV	SOS, eV	BR	L-WHM, eV		G-WHM, eV		AP
				$3d_{5/2}$	**$3d_{3/2}$**	**$3d_{5/2}$**	**$3d_{3/2}$**	
Rh^0	307.11	4.7	1.5	0.3	0.3	0.8	1.0	0.07
Rh^{3+}	308.21	4.7	1.5	0.4	0.4	1.0	1.4	0.00

S2. Crystallinity of Co_3O_4(111) film

An STM image obtained from the Co_3O_4(111) film grown on the Ir(100) substrate is shown in Figure S1. We observed well-ordered Co_3O_4(111) terraces terminated by Co^{2+} cations in agreement with literature.[S1, 2] On the clean surface, we detected an ordered atomic structure and specific structural features which appear as bright protrusions and a small fraction of dark

depressions. In our earlier work,[S2] we assigned the bright features to hydroxyl groups (OH^-) located on top of Co^{2+} cations with the hydrogen atom (H^+) on a nearby oxygen anion and dark features to Co^{2+} vacancies.

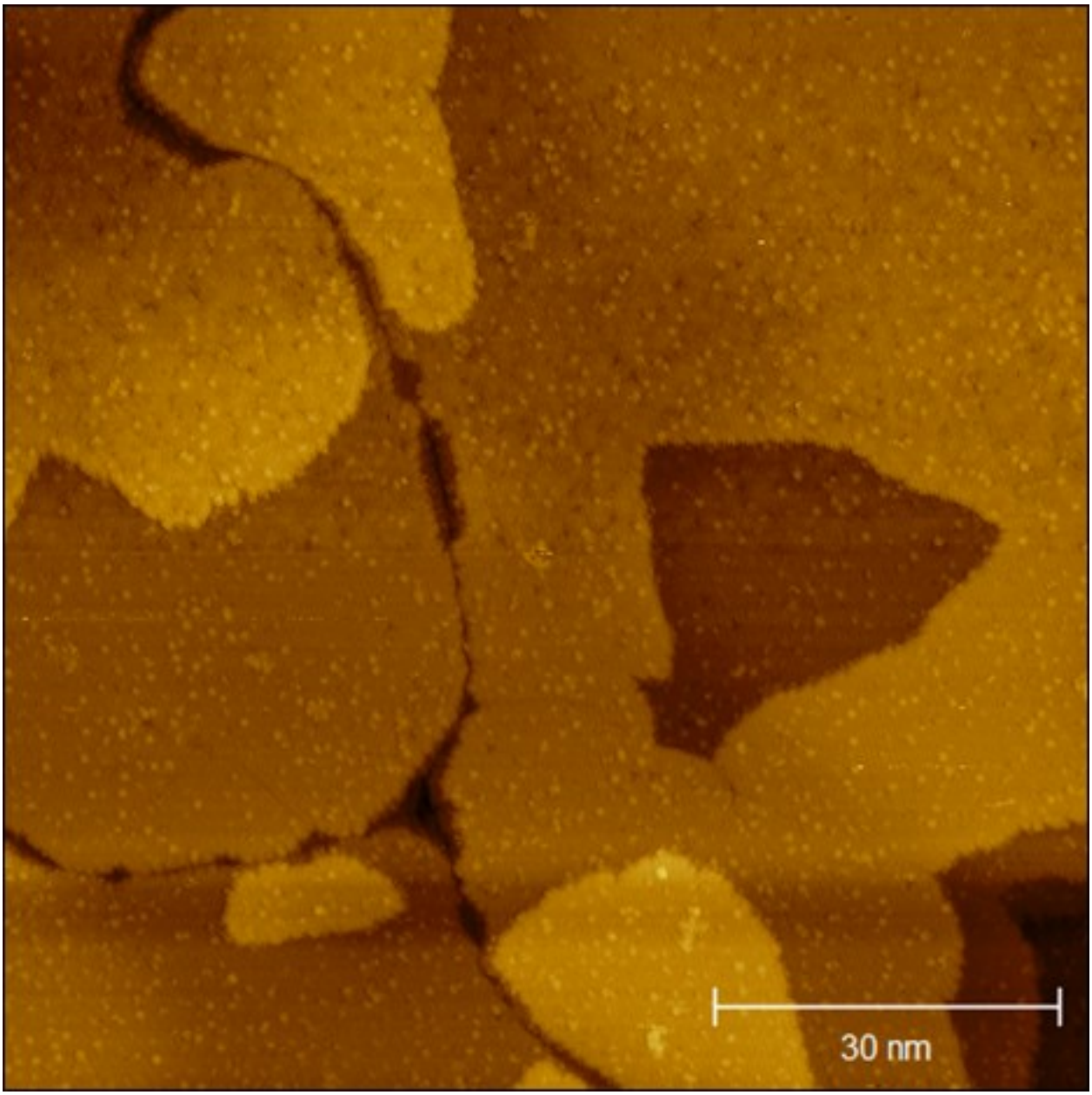

Figure S1. STM image obtained from the $Co_3O_4(111)$ film grown on the Ir(100) substrate.

S3. Depth profile of the Pd/Co_3O_4(111) model system

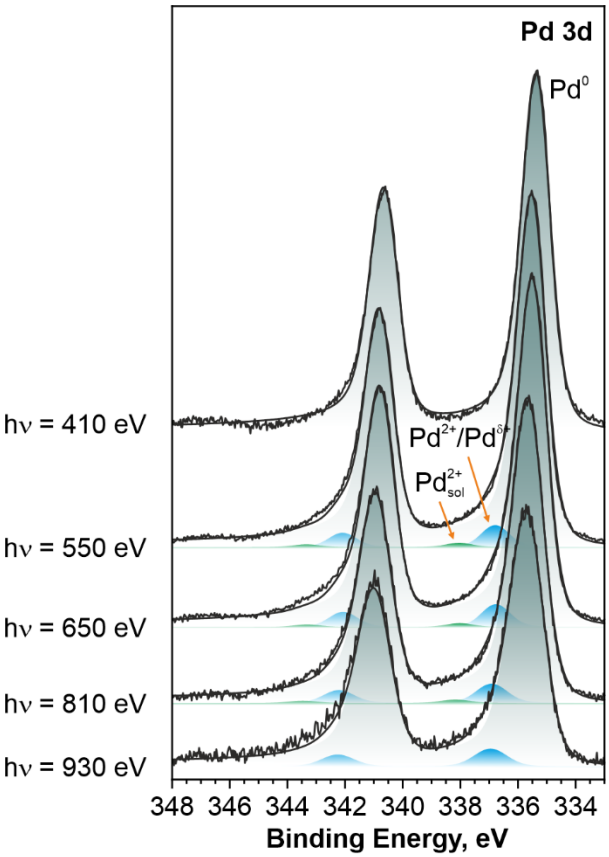

Figure S2. Pd 3d core level spectra obtained from Pd/Co_3O_4(111) with different photon energies. The spectra are normalized to area of unity.

S4. Estimation of the catalyst dissolution and carbon deposition by SRPES method

The fraction of the dissolved Pd atoms, X, and the thickness of carbon layer, d, can be estimated as follows:

$$X = \frac{N\times(e^{-\frac{d}{\lambda}\times I^{before}-I^{after}})}{e^{-\frac{d}{\lambda}\times I^{before}}} \qquad \text{(S1)},$$

where I^{before} and I^{after} are the total Pd 3d intensities obtained before and after the CV series, N is the total number of Pd atoms per surface area, λ is inelastic mean free path of the Pd 3d photoelectrons in carbon layer. λ is a function of the photon energy.

The idea of the analysis is to plot the X values as a function of photon energy. In the next step, the thickness of carbon layer, d, is selected until the differences between the X values are minimal (i.e.

a slope of the function approaches zero). The intercept of the plot corresponds to the average amount of dissolved metal.

We validated the corresponding method based on the data published in Ref. [S3], which were obtained by SRPES and online inductively coupled plasma-mass spectrometry (ICP-MS) from identical samples subjected to similar electrochemical treatments. More specifically, we determined the amounts of dissolved Pt after the immersion of 1.64 ML $Pt/Co_3O_4(111)$ into pure alkaline electrolyte (pH 10) at 0.5 V_{RHE}. The dissolution of the material observed during the contact is referred to as a contact peak is the Ref.[S3] We integrated the area of the contact peak measured by ICP-MS and found that the fraction of dissolved Pt was 0.44% with respect to the total initial amount of Pt in the sample.

To calculate the amount of dissolved metal based on SRPES method, we developed a Python script, shown below. The script uses a minimization algorithm based on the standard deviation function applied to the fractions of dissolved metal, *X*, by optimizing the thicknesses of carbon deposit *d*. The dispersion of the fractions of dissolved Pt atoms is plotted in Figure S3a for three different thicknesses of carbon deposit.

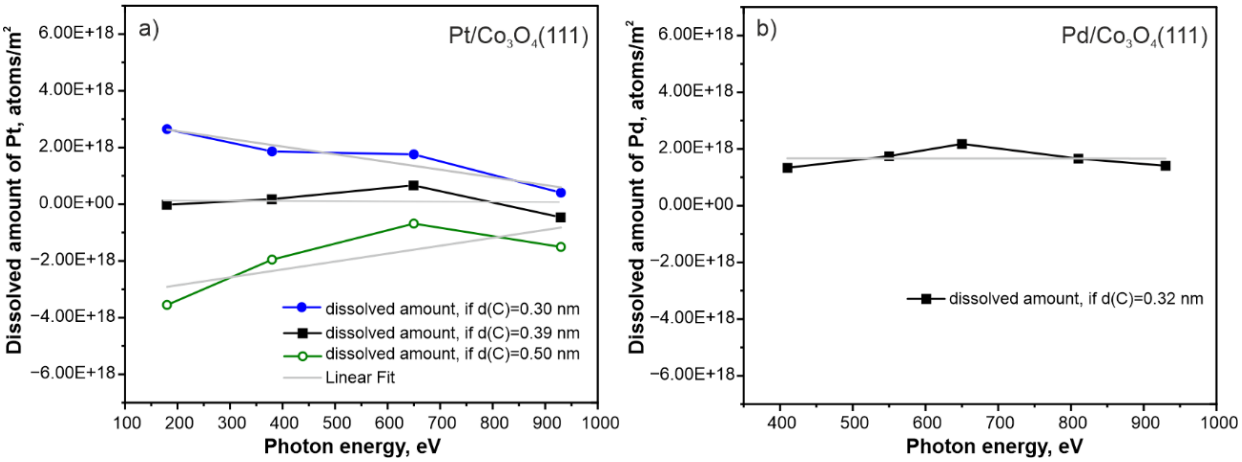

Figure S3. The fraction of dissolved noble metal atoms as determined by means of SRPES method on $Pt/Co_3O_4(111)$ (a) and $Pd/Co_3O_4(111)$ (b) samples after different electrochemical treatments (see text for more details).

Among these, the plot with a zero slope corresponds to the thickness of carbon deposit of 0.39 nm. The intercept of the corresponding plot gives the average fraction of dissolved Pt, which corresponds to about 0.36% with respect to the total initial amount of Pt in the sample. We conclude that the correspondence of the fractions of dissolved Pt determined by two different

methods is satisfactory. Generally, the accuracy of the SRPES method can be further improved by increasing the quality of the measured spectra, i.e. signal-to-noise ratio.

The fraction of dissolved Pd atoms determined by means of SRPES on the Pd/Co_3O_4(111) sample discussed in the present manuscript after the first CV series is plotted in Figure S3b. The calculated fraction of dissolved Pd after the first CV series is 7% for the thickness of carbon deposit of 0.31 nm.

The Python script is shown below. The code can be accessed at Zenodo: https://doi.org/10.5281/zenodo.14733690.

```python
import numpy as np
import matplotlib.pyplot as plt
from scipy.optimize import minimize

### ========== USER PARAMETERS ========== ###
photonEnergy = [180, 380, 650, 930] # Photon energies given in eV
inelasticMeanFreePath = [7.79, 12.5, 19.07, 25.51] # IMFP in Carbon at each photon energy given in A
intensityBeforeDissolution = [154124, 388258, 211069, 54654] # SRPES peak intensity before dissolution at each photon energy
intensityAfterDissolution = [93216, 281611, 167056, 47772] # SRPES peak intensity after dissolution at each photon energy
depositedLayerThickness = 3.6 # Average layer thickness given in A
depositedMetalDensity = 21450 # Bulk Density given in kg/m3
depositedMetalAtomMass = 3.23945e-25 # Atomic Mass given in kg

### ========== FUNCTION DECLARATION ========== ###
def calculateAtomsPerArea():
    """Calculate the number of atoms per square meter from global variables"""
    return depositedMetalDensity * depositedLayerThickness * 1e-10 / depositedMetalAtomMass

def calculateDissolvedAtoms(d):
    """Calculate the number of dissolved atoms from global variables and the thickness d"""
    dissolved = np.zeros(len(photonEnergy))
    for i in range(len(photonEnergy)):
        attIntensity = intensityBeforeDissolution[i] * np.exp(-d / inelasticMeanFreePath[i])
        dissolved[i] = atomsPerArea * (attIntensity - intensityAfterDissolution[i]) / attIntensity
    return dissolved

### ========== CALCULATION AND MINIMIZATION ========== ###
atomsPerArea = calculateAtomsPerArea()
result = minimize(lambda d: np.std(calculateDissolvedAtoms(d)), x0=10, tol=1e12)
optimizedD = result.x[0]
dissolvedAtomsPercentage = calculateDissolvedAtoms(optimizedD) / atomsPerArea * 100
dissolvedAtomsMeanPercentage = np.mean(dissolvedAtomsPercentage)

### ========== OUTPUT ========== ###
print(result)
print(f"Dissolved Atoms for each Photon Energy:\n{', '.join([f'{v:.5g}' for v in calculateDissolvedAtoms(optimizedD)])}")
print(f"Average Dissolved Atoms: {np.mean(calculateDissolvedAtoms(optimizedD)):.5g}\nTotal Atoms: {atomsPerArea:.5g}")
print(f"Calculated Thickness: d = {optimizedD:.5g} A\nDissolution Amount: {dissolvedAtomsMeanPercentage:.4g} %")
plt.figure(figsize = (9,6), dpi = 240)
plt.plot(photonEnergy, dissolvedAtomsPercentage, "oc-", label = "Calculated")
plt.plot(photonEnergy, [dissolvedAtomsMeanPercentage]*len(photonEnergy), color = "k", label = "Average")
plt.title("Dissolution Fit")
plt.xlabel("Photon Energy [eV]")
plt.ylabel("Dissolution [%]")
plt.legend()
plt.show()
```

S5. Binding energy shifts of Co 2p and O 1s core level spectra during experiments

The evolution of the Co 2p and O 1s core level spectra obtained from Rh/Co_3O_4(111) and Pd/Co_3O_4(111), and Rh@Pd/Co_3O_4(111) and Pd@Rh/Co_3O_4(111) before and after electrochemical experiments are shown in Figure S4 and Figure S5, respectively.

To follow the binding energy shift affected by the electrochemical conditions, we used the two most prominent peaks from as-prepared Co_3O_4(111) (bottom spectra in Figure S4a–d and Figure S5a–d): a Co 2p doublet peak associated with Co^{3+} atoms (light blue in Figure S4a–b and Figure S5a–b), and an O 1s peak associated with oxygen of the Co_3O_4 lattice (navy blue in Figure S4c–d and Figure S5c–d). For more detailed assignment of the Co 2p contributions, see our previous study.[S4]

In the monometallic Rh (Figure S4a,c) and Pd (Figure S4b,d) samples, emersion from the electrolyte after cyclic voltammetry (CV) in the range of 0.3–1.1 V_{RHE} resulted in no binding energy shift compared to the as-prepared Rh/Co_3O_4(111) and Pd/Co_3O_4(111) samples. After CV in the range of 0.3–1.5 V_{RHE} followed by CV in the range of 0.3–1.1 V_{RHE}, we observed binding energy shifts in the Co 2p and O 1s core levels of ~1 eV toward higher binding energies in the case of Rh/Co_3O_4(111) and 0.2 eV toward lower binding energies in the case of Pd/Co_3O_4(111).

In the Rh@Pd/Co_3O_4(111) sample after CV in the range of 0.3–1.1 V_{RHE} (Figure S5a,c), we observed binding energy shifts of 1.1 eV and 0.6 eV toward higher binding energies for the Co 2p and O 1s core level spectra, respectively. After CV in the range of 0.3–1.5 V_{RHE} followed by cycling in the range of 0.3–1.1 V_{RHE}, the spectra shifted by 0.2 eV toward lower binding energies. On the other hand, we observed only slight binding energy shifts toward higher binding energies in the Co 2p and O 1s core level spectra in Pd@Rh/Co_3O_4(111) – 0.2 (Co 2p) and 0.1 (O 1s) eV after CV in the range of 0.3–1.1 V_{RHE}, and 0.3 (Co 2p) and 0.1 (O 1s) eV after cycling in the range of 0.3–1.5 V_{RHE} followed by CV in the range of 0.3–1.1 V_{RHE}. (Figure S5b,d).

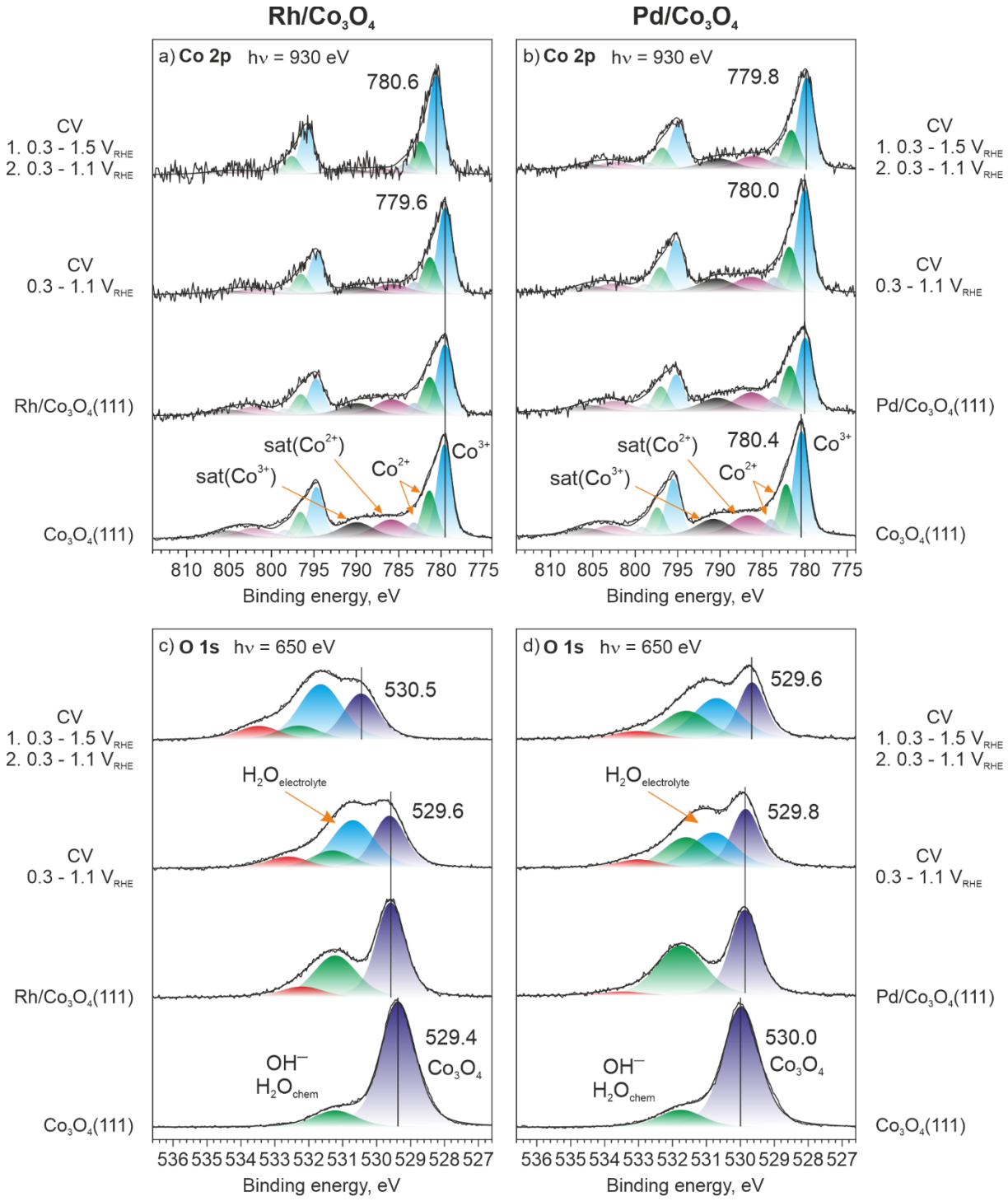

Figure S4. Co 2p (a, b) and O 1s (c, d) core level spectra obtained from $Rh/Co_3O_4(111)$ (a, c) and $Pd/Co_3O_4(111)$ (b, d) model catalysts before and after electrochemical experiments. The Co 2p and O 1s spectra were acquired with photon energies of 930 and 650 eV, respectively. The series of spectra are presented after normalization of the total peak areas to unity.

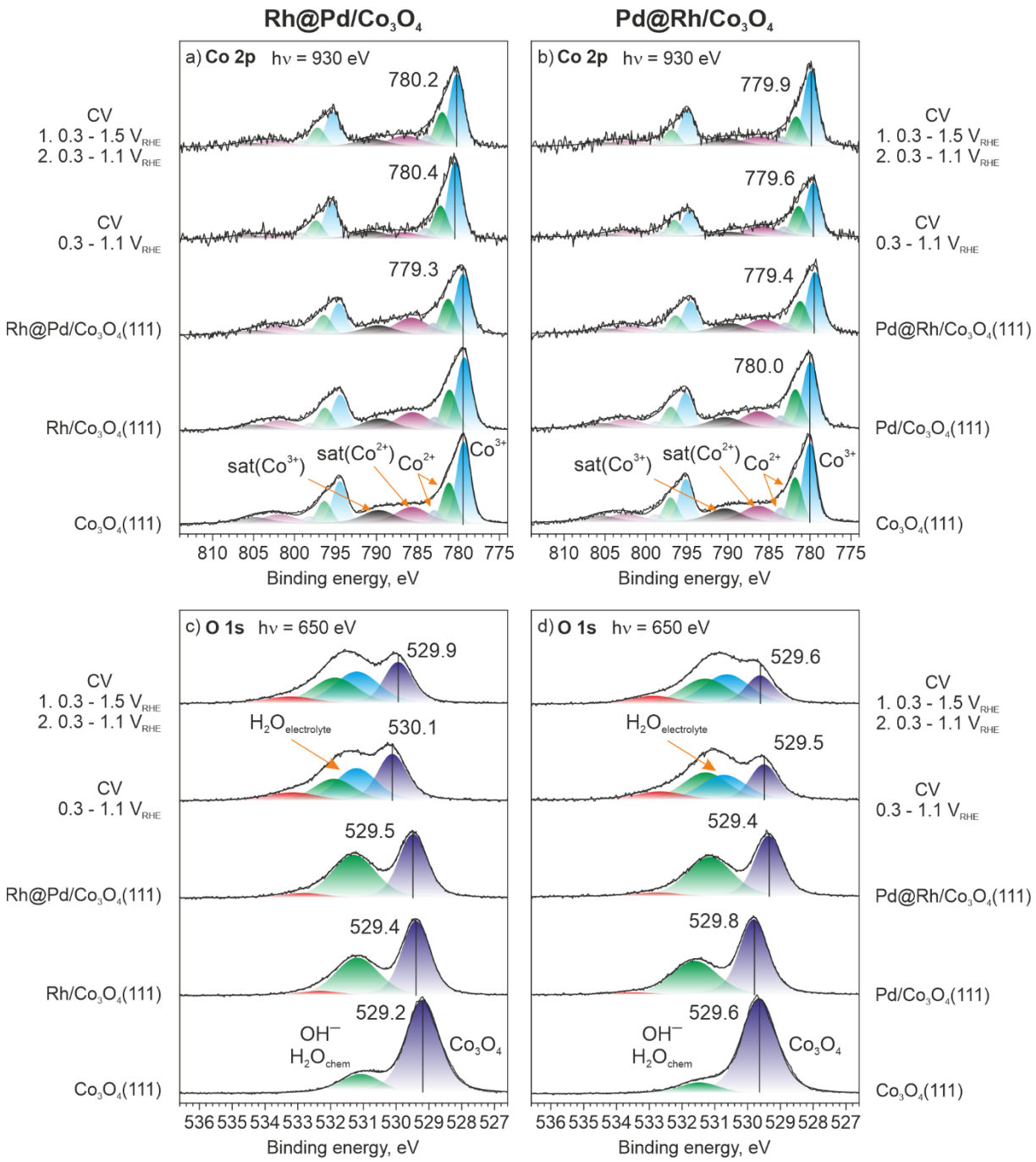

Figure S5. Co 2p (a, b) and O 1s (c, d) core level spectra obtained from Rh@Pd/Co_3O_4(111) (a, c) and Pd@Rh/Co_3O_4(111) (b, d) model catalysts before and after electrochemical experiments. The Co 2p and O 1s spectra were acquired with photon energies of 930 and 650 eV, respectively. The series of spectra are presented after normalization of the total peak areas to unity.

S6. Depth profile distribution of Rh oxidation states in Rh, Rh@Pd and Pd@Rh nanoparticles supported on $Co_3O_4(111)$

We have studied the distribution of Rh oxidation states as a function of information depth using photon energies between 410 and 930 eV. The information depth correlates with the inelastic mean free path (IMFP) of the photoelectrons and increases with increasing photon energy.[S5] The IMFPs of the Rh 3d electrons for the photon energies between 410 and 930 eV are given in Table S6. The Rh 3d core level spectra and the evolution of the integrated relative contributions of the Rh species obtained from depth profiling of $Rh/Co_3O_4(111)$, $Rh@Pd/Co_3O_4(111)$, and $Pd@Rh/Co_3O_4(111)$ samples before and after the electrochemical experiments are shown in Figure S6, Figure S7, and Figure S8, respectively.

Table S5. The inelastic mean free paths (IMFPs) of Rh 3d photoelectrons in $Co_3O_4(111)$, Pd and Rh as a function of photon energy.[S5]

Photon energy, eV	Rh 3d IMFP in $Co_3O_4(111)$, nm	Rh 3d IMFP in Pd, nm	Rh 3d IMFP in Rh, nm
410	0.52	0.40	0.40
550	0.73	0.55	0.55
650	0.90	0.67	0.67
810	1.15	0.86	0.86
930	1.34	0.99	0.99

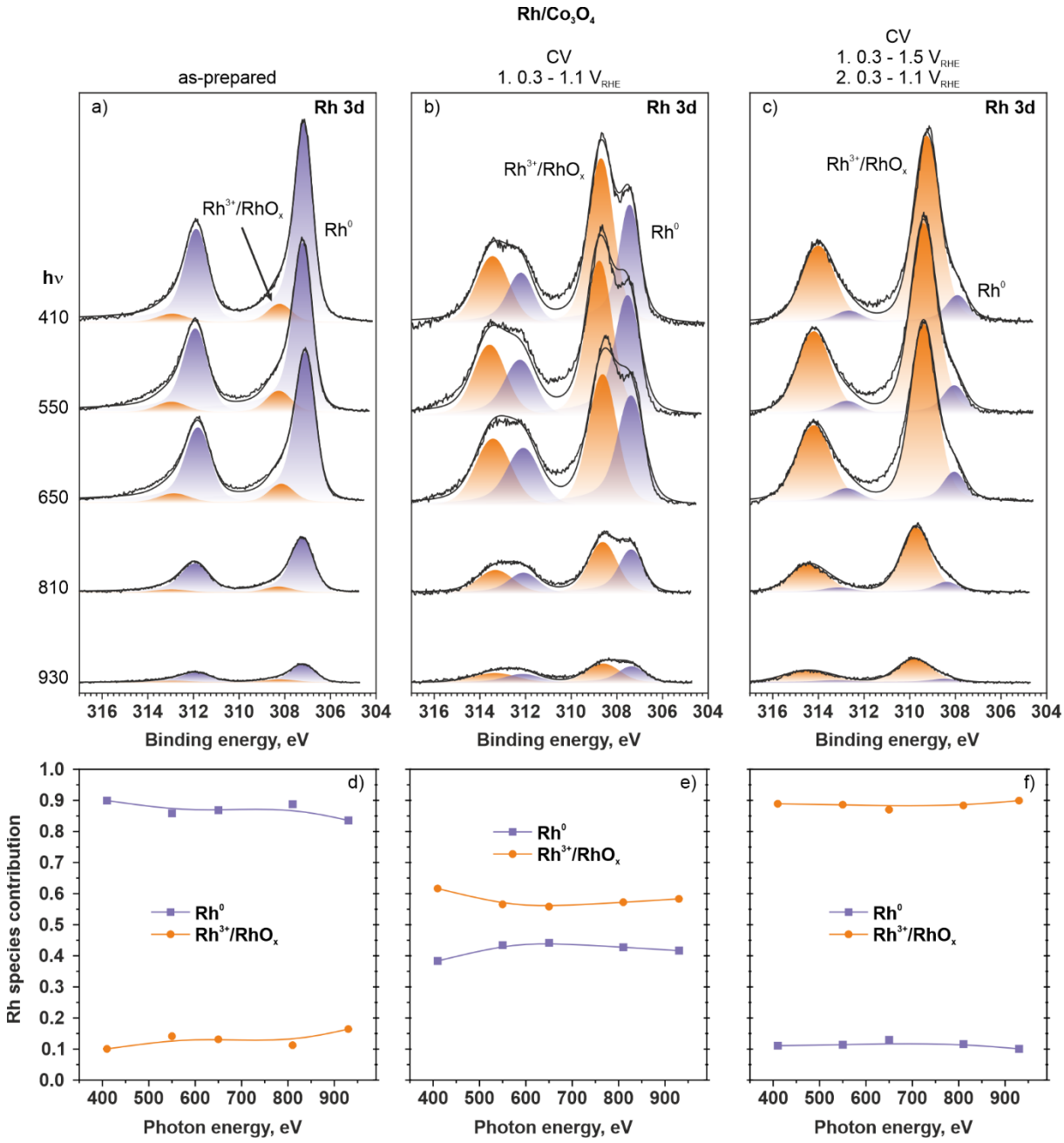

Figure S6. Rh 3d core level spectra (a–c) and the evolution of the integrated relative contributions of the Rh surface species (d–f) obtained from the Rh/Co_3O_4(111) model catalyst before and after electrochemical experiments. The Rh 3d spectra were acquired with photon energies between 410 and 930 eV.

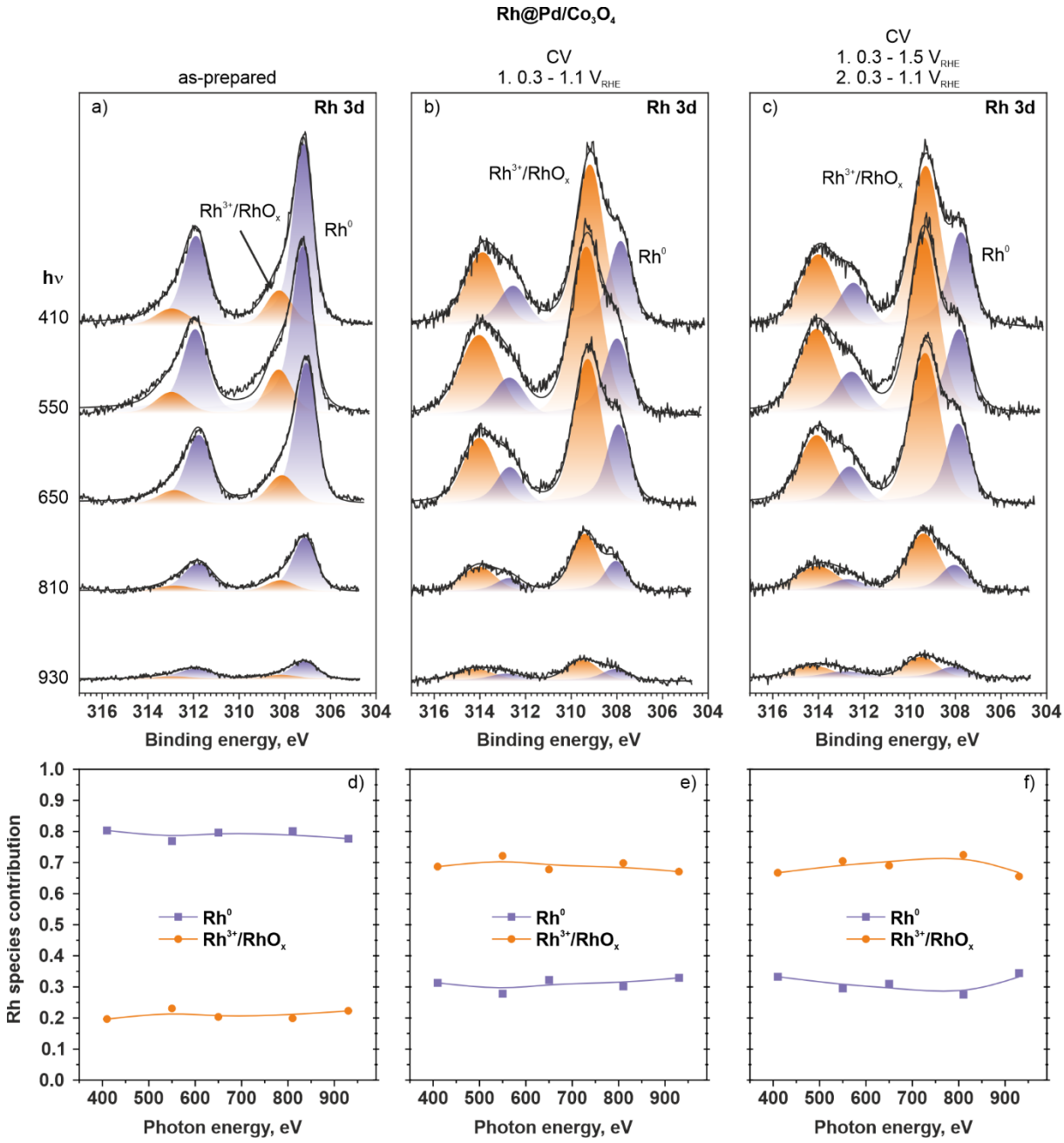

Figure S7. Rh 3d core level spectra (a–c) and the evolution of the integrated relative contributions of the Rh surface species (d–f) obtained from the Rh@Pd/Co_3O_4(111) model catalyst before and after electrochemical experiments. The Rh 3d spectra were acquired with photon energies between 410 and 930 eV.

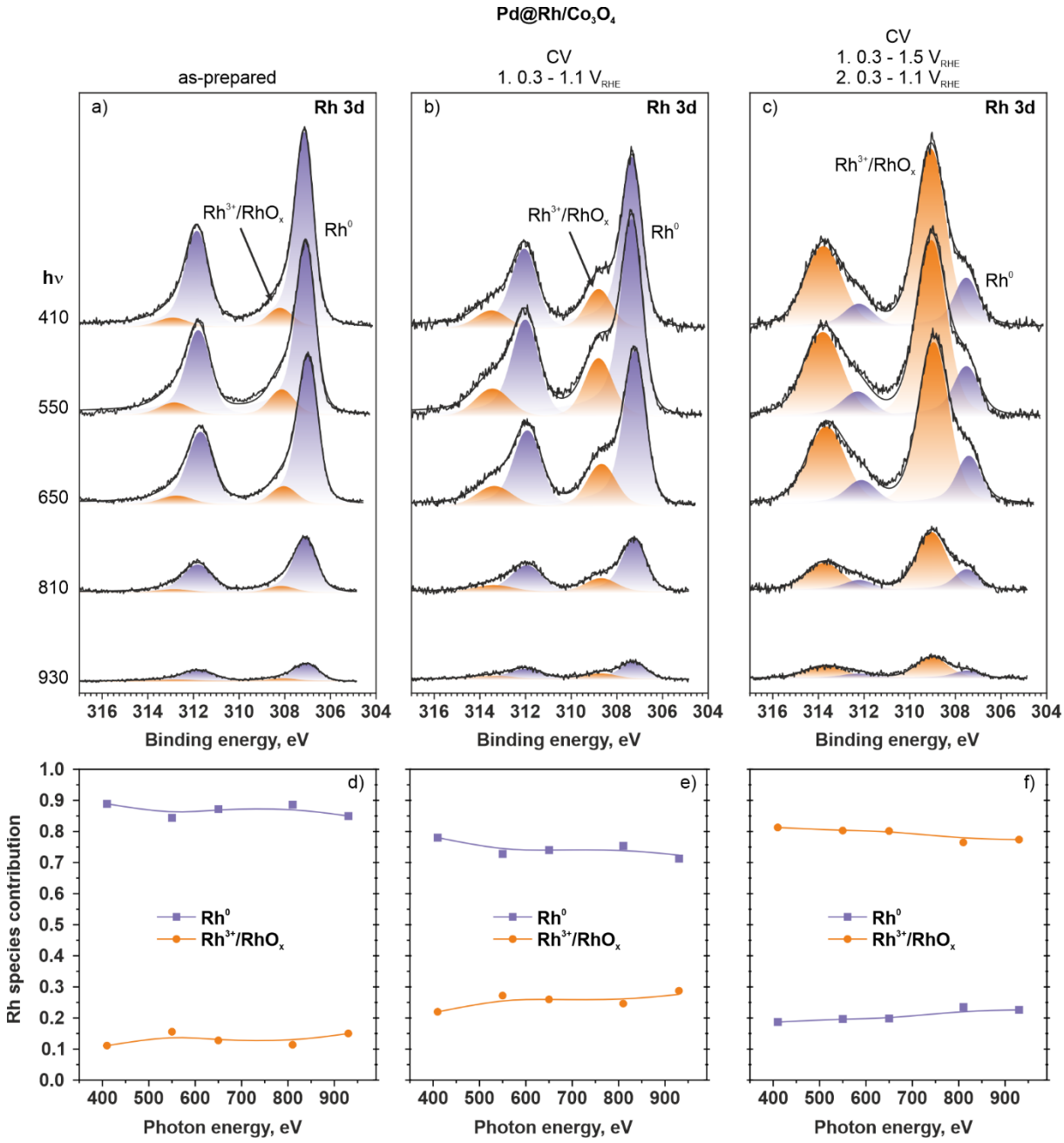

Figure S8. Rh 3d core level spectra (a–c) and the evolution of the integrated relative contributions of the Rh surface species (d–f) obtained from the Pd@Rh/Co_3O_4(111) model catalyst before and after electrochemical experiments. The Rh 3d spectra were acquired with photon energies between 410 and 930 eV.

References

S1. W. Meyer, K. Biedermann, M. Gubo, L. Hammer and K. Heinz, *J. Phys.: Condens. Matter*, 2008, **20**, 265011.

S2. L. Fusek, M. Farnesi Camellone, M. Ronovský, M. Kastenmeier, T. Skála, P. K. Samal, N. Tsud, S. Mehl, J. Škvára, T. Dolák, V. Uvarov, M. Setvín, V. Johánek, S. Fabris, O. Brummel, J. Libuda, J. Mysliveček, S. Piccinin and Y. Lykhach, *J. Mater. Chem. A*, 2024, **12**, 3258-3264.

S3. M. Bertram, C. Prössl, M. Ronovský, J. Knöppel, P. Matvija, L. Fusek, T. Skála, N. Tsud, M. Kastenmeier, V. Matolín, K. J. J. Mayrhofer, V. Johánek, J. Mysliveček, S. Cherevko, Y. Lykhach, O. Brummel and J. Libuda, *J. Phys. Chem. Lett.*, 2020, **11**, 8365–8371.

S4. Y. Lykhach, S. Piccinin, T. Skála, M. Bertram, N. Tsud, O. Brummel, M. Farnesi Camellone, K. Beranová, A. Neitzel, S. Fabris, K. C. Prince, V. Matolín and J. Libuda, *J. Phys. Chem. Lett.*, 2019, **10**, 6129-6136.

S5. S. Tanuma, C. J. Powell and D. R. Penn, *Surf. Interface Anal.*, 1994, **21**, 165-176.